

Geometric Fabrics for the Acceleration-based Design of Robotic Motion

Mandy Xie^{*1,2}, Karl Van Wyk^{*1}, Anqi Li^{1,3}, Muhammad Asif Rana^{1,2},
Dieter Fox^{1,3}, Byron Boots^{1,3}, and Nathan Ratliff¹

Abstract—This paper describes the pragmatic design and construction of geometric fabrics for shaping a robot’s task-independent nominal behavior, capturing behavioral components such as obstacle avoidance, joint limit avoidance, redundancy resolution, global navigation heuristics, etc. Geometric fabrics constitute the most concrete incarnation of a new mathematical formulation for reactive behavior called optimization fabrics. Fabrics generalize recent work on Riemannian Motion Policies (RMPs); they add provable stability guarantees and improve design consistency while carrying forward the intuitive acceleration-based principles of modular design that make RMPs successful. We describe a suite of mathematical modeling tools that practitioners can employ in practice and demonstrate both how to mitigate system complexity by constructing behaviors layer-wise and how to employ these tools to design robust strongly-generalizing policies that solve practical problems one would expect to find in industry applications. Our experimental system exhibits intelligent global navigation behaviors expressed entirely as fabrics with zero planning or state machine governance.

I. INTRODUCTION

Motion generation is one of the fundamental problems of robotics. Fast, reactive, motion is essential for most modern tasks, especially in highly-dynamic and uncertain collaborative environments. In this paper, we describe a set of tools for the direct construction of robotic behavior in modular parts. Specifically, we show how to design *geometric fabrics* and present a collection of pragmatic tools building on the recent theory of *optimization fabrics* detailed in [1]. The term *fabric* is used analogously to the term *fabric of spacetime* from theoretical physics, but formalizes the idea as a second-order nonlinear differential equation characterizing an *unbiased* nominal behavior. That nominal behavior exists independent of a specific task and is shared by multiple tasks; a given task is then defined as

an optimization problem within the fabric wherein the task goal is to optimize a potential function. The fabric acts to shape the behavior of the optimization path en route toward the minimum.

For instance, the goal of a given task may be to reach a target point with the robot’s end-effector. However, en route, the system should avoid obstacles and joint limits, resolve redundancy intelligently, implement global navigation heuristics, and may even need to shape the end-effector path to approach the target from a specific direction. The task is the optimization problem characterizing the end-effector’s target; the fabric captures everything else about the behavior we want the robot to exhibit en route.

Geometric fabrics are a special type of fabric that expresses this unbiased nominal behavior as a generalized nonlinear geometry in robot’s configuration space. We will show that a wide range of robotic behavior can be captured purely by its geometric fabric, including those listed above. We detail a pragmatic collection of modeling tools derived from this framework, and present experimental results on a Franka Panda robotic manipulator fluently navigating furniture mimicking problems common in logistics or industrial settings.

Importantly, geometric fabrics are a class stable RMPs. In [1] (Section I.A), we describe in detail the theoretical limitations of earlier stable frameworks for RMPs [2, 3, 4, 5] which we know as the subclass of *Lagrangian* fabrics within the context of our new theory. In this paper we show how those limitations manifest practically in direct comparisons to geometric fabrics (see Section VII). In addition to their stability, geometric fabrics encode behavior as speed-invariant paths which manifests as a geometric consistency when modular parts are combined, and they retain the intuitive character acceleration-based design that makes canonical-form RMPs powerful.

*Equal contribution

¹All authors are with (or interned at) NVIDIA

²Georgia Tech

³University of Washington

A. Related work

Much of the classical literature on robotic motion generation focuses on discrete planning queries [6]. Recent work by [7] observed that there’s a push and pull between modeling fidelity and computational expense for most modern continuous time re-planning systems, including those built on state-of-the-art optimization techniques [8, 9, 10]—many research implementations simplify the problem considerably to achieve the speeds they do. As such, real-time reactive motion building on classical tools such as Operational Space Control [4], were proposed by [7] as a fundamental building block of modern collaborative system design.

A new line of research around Riemannian Motion Policies (RMPs) [11, 2] addressing how to empower these reactive motion frameworks to exhibit more globally aware behaviors, such as obstacle avoidance, grew from that observation and led to some impressive strongly-generalizing systems¹ using RMPs as building blocks and circumventing standard planning architectures entirely.

Optimization fabrics [1] are the culmination of that line of work into a comprehensive mathematical theory of behavioral design with rigorous stability guarantees. And geometric fabrics, described here, are the most concrete incarnation of those tools. Earlier systems designed around RMPs orchestrated behaviors using (at times complex) state machines that supplemented RMPs with higher-level task choices such as way-point or standoff-point targeting. Work on learning RMPs [12, 13, 14] aimed to address the challenge of designing intuitive but highly nonlinear behaviors, but the resulting policies had trouble integrating with existing RMP systems. Within the context of optimization fabrics [1], we now know these limitations stem from the use of classical mechanical systems (more generally the family of Lagrangian fabrics) as the behavioral model, which suggests future exploration into learning more flexible fabrics, such as geometric fabrics, may be promising.

II. PRELIMINARIES

Geometric fabrics build on the theory of spectral semi-sprays (specs), detailed in our companion theoretical paper [1], which generalize the idea of modular second-order differential equations first derived

¹Systems designed and tested on a collection of validation examples that then perform robustly on an entire distribution of problems.

and used as Riemannian Motion Policies (RMPs) in [11, 2]. We focus on second-order representations of policies to fully model the capabilities and dynamical considerations of physical manipulators, which themselves are modeled as second-order differential equations.

Let \mathcal{C} be the d -dimensional configuration space of the robot.² Throughout this paper, we will use vector-notation describing elements of a space in coordinates. Mapped task spaces $\mathbf{x} = \phi(\mathbf{q})$ are defined in coordinates³ $\phi : \mathbb{R}^d \rightarrow \mathbb{R}^n$ with Jacobian matrix $\mathbf{J} = \partial_{\mathbf{x}}\phi$, used in the relations $\dot{\mathbf{x}} = \mathbf{J}\dot{\mathbf{q}}$ and $\ddot{\mathbf{x}} = \mathbf{J}\ddot{\mathbf{q}} + \dot{\mathbf{J}}\dot{\mathbf{q}}$.

The spec algebra enables the construction of transform trees of task spaces that can be populated by specs representing parts of a differential equation. Through the algebraic operations of spec summation and pullback, following [2, 1], the tree implicitly represents a complete differential equation at the root as a sum of the parts. Natural-form specs $(\mathbf{M}, \mathbf{f})_{\mathcal{X}}$ represent equations of the form $\mathbf{M}(\mathbf{x}, \dot{\mathbf{x}})\ddot{\mathbf{x}} + \mathbf{f}(\mathbf{x}, \dot{\mathbf{x}}) = \mathbf{0}$, and their algebra is derived based on the formulas how these equations sum transform to other spaces under $\ddot{\mathbf{x}} = \mathbf{J}\ddot{\mathbf{q}} + \dot{\mathbf{J}}\dot{\mathbf{q}}$. We refer to [1] for explicit expressions. Often a canonical-form spec $(\mathbf{M}, \mathbf{h})_{\mathcal{X}}^{\mathcal{C}}$, where $\mathbf{h} = \mathbf{M}^{-1}\ddot{\mathbf{x}}$ is used to express the acceleration-form equation $\ddot{\mathbf{x}} + \mathbf{h}(\mathbf{x}, \dot{\mathbf{x}}) = \mathbf{0}$. For robotics applications we find it useful to additionally introduce a *policy-form* spec $[\mathbf{M}, \pi]_{\mathcal{X}}$ to denote the solved policy expression $\ddot{\mathbf{x}} = -\mathbf{h}(\mathbf{x}, \dot{\mathbf{x}}) = \pi(\mathbf{x}, \dot{\mathbf{x}})$. Aside from the negated $\pi = -\mathbf{h}$ the algebra and semantics is otherwise the same.⁴ The policy form makes it easier to think of the spec as an *acceleration policy* π with associated priority metrics \mathbf{M} .

As in [2] these differential equations can easily be executed on fully actuated robotic systems using standard control techniques such as feedback linearization. For instance, a straightforward method is to use policies as trajectory generators (integrate forward integral curves) and follow those in the

²By convention, we use \mathbf{q} to denote configurations in the configuration space \mathcal{C} . For all other space, we denote elements of a given space using bold lower case version of the upper case script letter representing task space name, such as $\mathbf{x} \in \mathcal{X}$.

³The spec algebra defines covariant transforms, so curvilinear changes of coordinates can be applied with no change to the behavior, in particular when moving across different coordinate charts of a manifold [15].

⁴The notation has been fluctuating in earlier papers on RMPs [11, 2]. Here we establish concretely that (\cdot, \cdot) expressions represent differential equations forms, and $[\cdot, \cdot]$ denote policy semantics.

physical system using PID control, as has been done in related work such as [16].

III. THEORETICAL GEOMETRIC TOOLS

For the derivation of geometric fabrics given in [1] it's important to know the theory of generalized nonlinear geometry and Finsler energy, but for their application in design it's sufficient to know just a few key facts. Here we give the critical information; for an in-depth exposition see [17].

A. Generalized nonlinear geometries

A generalized nonlinear geometry is an acceleration policy $\ddot{\mathbf{x}} = \pi(\mathbf{x}, \dot{\mathbf{x}})$ for which π has a special homogeneity property. We require that it be *positively homogeneous of degree 2* (HD2), which means that for any $\lambda \geq 0$ we have $\pi(\mathbf{x}, \lambda\dot{\mathbf{x}}) = \lambda^2\pi(\mathbf{x}, \dot{\mathbf{x}})$. One can show that the HD2 property ensures the differential equation is more than just a collection of trajectories (its integral curves); it additionally has a *path consistency* property whereby every integral curve starting from a given position \mathbf{x}_0 with velocity $\dot{\mathbf{x}}_0 = \eta\hat{\mathbf{n}}$ pointing in a given direction $\hat{\mathbf{n}}$ (here $\eta > 0$) will follow *the same* path [17]. In particular, any variant of the differential equation of the form $\ddot{\mathbf{x}} = \pi(\mathbf{x}, \dot{\mathbf{x}}) + \alpha(t, \mathbf{x}, \dot{\mathbf{x}})\dot{\mathbf{x}}$, where $\alpha \in \mathbb{R}$, will have integral curves that trace out the same paths as π . That geometric consistency property turns π into what we call a *geometry of paths*.

B. Finsler energies

A Finsler energy $\mathcal{L}_e(\mathbf{x}, \dot{\mathbf{x}})$ is a generalization of classical kinetic energy from classical mechanics (the classical kinetic energy $\mathcal{K} = \frac{1}{2}\dot{\mathbf{x}}^T\mathbf{G}(\mathbf{x})\dot{\mathbf{x}}$ is a form of Finsler energy). Analogous to the classical case, through the Euler-Lagrange equation, a Finsler energy defines an equation of motion $\mathbf{M}_e(\mathbf{x}, \dot{\mathbf{x}})\ddot{\mathbf{x}} + \mathbf{f}_e(\mathbf{x}, \dot{\mathbf{x}}) = \mathbf{0}$ where $\mathbf{M}_e = \partial_{\dot{\mathbf{x}}}^2\mathcal{L}_e$ is known as the *energy (or metric) tensor* and $\mathbf{f}_e = \partial_{\dot{\mathbf{x}}\dot{\mathbf{x}}}\mathcal{L}_e\dot{\mathbf{x}} - \partial_{\mathbf{x}}\mathcal{L}_e$ captures curvature terms (Coriolis and centripetal forces in classical mechanics). This equation matches the classical mechanical equations of motion when $\mathcal{L}_e = \mathcal{K}$, for which $\mathbf{M}_e(\mathbf{x}, \dot{\mathbf{x}}) = \mathbf{G}(\mathbf{x})$.

In geometric fabrics, the energy tensor defines the policy's *priority metric* and the curvature terms \mathbf{f}_e are used to ensure stability (see Section VI-C). See [17] for an in-depth review of Finsler geometry. Here, we just need to know that Finsler energies are Lagrangian functions $\mathcal{L}_e(\mathbf{x}, \dot{\mathbf{x}})$ satisfying

- 1) Positivity: $\mathcal{L}_e(\mathbf{x}, \dot{\mathbf{x}}) \geq 0$ with equality only when $\dot{\mathbf{x}} = \mathbf{0}$.
- 2) Homogeneity: $\mathcal{L}_e(\mathbf{x}, \dot{\mathbf{x}})$ is positively homogeneous of degree 2 in $\dot{\mathbf{x}}$; i.e. for $\lambda \geq 0$ we have $\mathcal{L}_e(\mathbf{x}, \lambda\dot{\mathbf{x}}) = \lambda\mathcal{L}_e(\mathbf{x}, \dot{\mathbf{x}})$.
- 3) Energy tensor invertibility: $\mathbf{M}_e = \partial_{\dot{\mathbf{x}}}^2\mathcal{L}_e$ is everywhere invertible.

The metric tensor $\mathbf{M}_e(\mathbf{x}, \dot{\mathbf{x}})$ is in general a function of *velocity* as well as position, although the above homogeneity requirement enforces that \mathbf{M}_e depends only on the *directionality* of the velocity ($\mathbf{M}_e(\mathbf{x}, \dot{\mathbf{x}}) = \mathbf{M}_e(\mathbf{x}, \hat{\dot{\mathbf{x}}}$ for $\dot{\mathbf{x}} \neq \mathbf{0}$) and not the magnitude (it is homogeneous of degree 0). This dependence on directionality enables us to design intuitive directionally dependence priority matrices in Section VI using Finsler energies.

IV. GEOMETRIC FABRICS

Geometric fabrics are a form of *optimization fabric* [1] which are a special type of nonlinear second-order differential equation that expresses a nominal behavior on a space designed to influence the optimization path of a differential optimizer. Specifically, when the fabric is *forced* away from its nominal trajectory by the negative gradient of an objective function (forcing potential), the theory of optimization fabrics guarantees that the resulting system will converge to a local minimum of the optimization problem defined by that objective. We don't dwell on the theory here (see [1] for that), but instead describe in detail pragmatically how to design the fabric to capture a collection of desired task-independent nominal behaviors and how to construct an intuitive forcing potential for over the top of that for to implement a task.

A *forced geometric fabric* is composed of a collection of *fabric terms* which are pairings $(\mathcal{L}_e, \pi)_{\mathcal{X}}$ between a Finsler energy and an acceleration policy. There are geometric terms constructing the geometric fabric, itself, and forcing terms defining the objective potential. A *geometric term* on a space \mathcal{X} is a fabric term $(\mathcal{L}_e, \pi_2)_{\mathcal{X}}$, matching an HD2 generalized nonlinear geometric acceleration policy $\ddot{\mathbf{x}} = \pi_2(\mathbf{x}, \dot{\mathbf{x}})$ to a Finsler energy $\mathcal{L}(\mathbf{x}, \dot{\mathbf{x}})$. A *forcing term* on \mathcal{X} , likewise, is a fabric term $(\mathcal{L}_e, -\mathbf{M}_e^{-1}\partial_{\mathbf{x}}\psi)_{\mathcal{X}}$ matching a Finsler energy \mathcal{L}_e to a forcing policy $-\mathbf{M}_e^{-1}\partial_{\mathbf{x}}\psi$ defined by a potential function $-\partial_{\mathbf{x}}\psi$. In general, many such fabric terms can be added to different spaces of a transform tree [2] for the modular design of composite behaviors.

Through the Euler-Lagrange equation $\mathbf{M}_e \ddot{\mathbf{x}} + \mathbf{f}_e = \mathbf{0}$ (see [17]), we can understand each fabric term as a triple $\mathcal{F} = (\mathbf{M}_e, \mathbf{f}_e, \pi)_{\mathcal{X}}$, or equivalently two specs, a policy form spec $\mathcal{G} = [\mathbf{M}_e, \pi]_{\mathcal{X}}$ and a natural form energy spec $\mathcal{E} = (\mathbf{M}_e, \mathbf{f}_e)_{\mathcal{X}}$. The algebra of geometric fabric summation and pullback is defined as the corresponding summation and pullback operations of the constituent specs $\mathcal{S}_e, \mathcal{S}_g$.

We can always summarize the resulting summed and/or pulled-back fabric term as its corresponding pairwise form (\mathcal{L}_e, π) . Doing so enables deriving direct expressions for the geometric fabric algebra on the pair representation. However, that's used just conceptually below, so we focus on the two-spec representation here.

A geometric fabric is a type of optimization fabric [1] and acts as an unbiased optimization medium. The theory dictates we can optimize any objective over the fabric by forcing it with the negative gradient of a smooth potential and choosing appropriate amount of damping (see Section V). This theory separates the design of a task-independent nominal behavior expressed by the fabric (represented by the geometric terms) from the task-specific objective (represented by the forcing terms). See Section VI for an overview of specific geometric fabric designs including boundary conforming terms for modeling obstacles and joint limits.

When designing a forced geometric fabric we follow the same intuition as designing RMPs [11], i.e. we construct it so that the policy specs $\mathcal{G} = [\mathbf{M}_e, \pi]_{\mathcal{X}}$ model the desired behavior, and we do so in parts understanding that the final behavior will be a metric-weighted average of the parts. Specifically, the acceleration policy π should define how we want the system to accelerate in that space, and the metric \mathbf{M}_e should be seen as an independently designed spectral weight matrix that defines how the policy should combine with other policies (colloquially, what directions in the space the policy cares about). The metric \mathbf{M}_e is HD0 as observed in Section III-B, so for the policy specs of geometric terms, since π_2 is an HD2 geometry, the metric-weighted average implementing policy spec summation results in an acceleration policy which is, itself, HD2 and hence a generalized nonlinear geometry thereby forming a consistent geometry of paths. The second spec in each fabric term, energy spec $\mathcal{E} = (\mathbf{M}_e, \mathbf{f}_e)_{\mathcal{X}}$, is used only to guarantee stability during execution (see Section V). Practitioners should focus on designing the behavior of the policy specs $[\mathbf{M}_e, \pi]$

when designing a fabric terms.

V. EXECUTION AND ALGORITHMS

The final step in executing a forced geometric fabric is speed modulation. We can drive the system through the fabric at any desired speed, as long as a specific lower bound on the required damping is met. Since geometric paths are independent of speed, speed control is particularly useful for geometric fabrics. We follow the speed control methodology outlined in [1] with specific functional forms described in Section VI-C.

The obtained differential equation can be integrated with respect to time using various integration methods. We have found that a good balance between integration speed and accuracy can be met with explicit Euler with a 1 ms time step or fourth order Runge-Kutta with a maximum time step of 10 ms. Other integration methods are useful as well like symplectic Euler or trapezoidal rule.

In full, we design a system in three parts: (1) design the underlying behavioral fabric, (2) add a driving potential to implement a task, (3) design an execution energy or speed control. All three parts leverage transform trees [2] of related task spaces as described next:

Design of a forced geometric fabric:

- 1) Construct a transform tree.
- 2) Populate its nodes with fabric terms. Most terms are geometric terms and just a few (often only one) are forcing terms.
- 3) Add execution energy specs to the tree as needed to describe the execution energy we want to control.

Execution of the forced fabric with speed control:

- 1) Forward pass: Populate the nodes with current state from the root to the leaves.
- 2) Backward pass: Evaluate the specs an pull them to root in separate channels, an *energy channel* for the geometric terms' energy specs, a *policy channel* for the geometric terms' policy specs, an *execution energy channel* for the execution energy specs, and a *forcing policy channel* for the forcing terms' policy specs. Add the forcing term's energy specs to the energy channel.
- 3) Use four channels' combined root results to calculate the final desired acceleration using speed control.

VI. CONCRETE DESIGN TOOLS

Here we review practical techniques for geometric fabric design.

Geometric fabrics follow acceleration-based design principles captured in the original canonical-form RMPs [11]. As described in Section IV, a geometric fabric is a pair $(\mathcal{L}_e, \pi_2)_{\mathcal{X}}$ characterizing two specs, an energy spec and a geometry spec. The energy spec captures stability information, while the geometry spec captures behavior. Behavioral design, therefore, focuses on constructing the latter, using the class of HD2 geometries to model π_2 and deriving \mathbf{M}_e as the energy tensor of a Finsler geometry \mathcal{L}_e .

When geometric fabrics are summed $\sum_i (\mathcal{L}_e^{(i)}, \pi_2^{(i)})_{\mathcal{X}}$, the combined fabric's geometry spec (capturing its behavior) $\sum_i (\mathbf{M}_e^{(i)}, \pi_2^{(i)})_{\mathcal{X}} = (\widetilde{\mathbf{M}}_e, \widetilde{\pi}_2)$ is a metric-weighted average of the contributing geometries $\widetilde{\pi}_2 = (\sum_i \mathbf{M}_e^{(i)})^{-1} \sum_i \mathbf{M}_e^{(i)} \pi_2^{(i)}$, prioritized by the total metric $\widetilde{\mathbf{M}}_e = \sum_i \mathbf{M}_e^{(i)}$. When populating a transform tree, this intuitive combination rule is applied recursively at each node. Designers need only focus on intuitively creating modular acceleration policies (as HD2 geometries) in the different spaces and prioritizing them with metric tensors (from Finsler energies) expressing how they should weigh against one another.

A. Construction of HD2 Geometries

An HD2 geometry is a differential equation $\ddot{\mathbf{x}} + \mathbf{h}_2(\mathbf{x}, \dot{\mathbf{x}}) = \mathbf{0}$ where \mathbf{h}_2 is HD2 (see Section III-A), which we usually denote in *policy* form $\ddot{\mathbf{x}} = -\mathbf{h}_2(\mathbf{x}, \dot{\mathbf{x}}) = \pi_2(\mathbf{x}, \dot{\mathbf{x}})$. Constructing an HD2 geometry is straightforward given the following rules of homogeneous functions: (1) a sum of HD2 functions is HD2; (2) multiplying homogeneous functions adds their degrees (denoting an HD k function as f_k , examples are $f_2 f_0 = f_2$, $f_1 f_1 = f_2$, etc.). For instance, a simple way to design an HD2 geometry is to choose an HD0 policy $\pi_0(\mathbf{x})$ that depends only on position and form $\pi_2(\mathbf{x}, \dot{\mathbf{x}}) = \|\dot{\mathbf{x}}\|^2 \pi_0(\mathbf{x})$ by scaling it by HD2 function $\|\dot{\mathbf{x}}\|^2$. That position dependent policy can be expressed as the negative gradient of a potential $\pi_0(\mathbf{x}) = -\partial_{\mathbf{x}} \psi(\mathbf{x})$, although it need not be.

B. Acceleration-based Potentials

It is often most intuitive to design a geometric fabrics' forcing potential as a forcing *spec* $\mathcal{F} = [\mathbf{M}_f, \pi_f]_{\mathcal{X}}$ in *policy form* so it's treated

intuitively as another acceleration policy averaged into the final metric weighted average. This policy π_f must, therefore, implicitly express a *forcing potential* $\psi_f(\mathbf{x})$ whose negative gradient is given by $-\partial_{\mathbf{x}} \psi_f(\mathbf{x}) = \mathbf{M}_f \pi_f$. When designing \mathcal{F} we must enforce that \mathbf{M}_f and π_f remain theoretically compatible in that sense. Following Appendix D.4 in [18], we advocate choosing $\pi_f = -\nabla_{\mathbf{x}} \psi_{\text{acc}}(\mathbf{x})$ where ψ_{acc} is a potential function that is spherically symmetric (isotropic) around its global minimum expressing the acceleration policy directly as its negative gradient. It can be shown that any metric $\mathbf{M}_f(\mathbf{x})$ dependent only on position is theoretically compatible per this requirement if it is also spherically symmetric (isotropic) around the same global minimum point. Note that position-only metrics are Riemannian and derive from Finsler energies of the form $\mathcal{L}_e = \frac{1}{2} \dot{\mathbf{x}}^T \mathbf{M}_f(\mathbf{x}) \dot{\mathbf{x}}$.

C. Speed control

We follow the speed control methodology outlined in [1]. Specifically, that entails using $\alpha_{\text{reg}} = \alpha_{\text{ex}}^{\eta} - \beta_{\text{reg}}(\mathbf{x}, \dot{\mathbf{x}}) + \alpha_{\text{boost}}$ in $\ddot{\mathbf{x}} = -\mathbf{M}_e^{-1} \partial_{\mathbf{x}} \psi(x) + \pi_0(\mathbf{x}, \dot{\mathbf{x}}) + \alpha_{\text{reg}} \dot{\mathbf{x}}$ with $\beta_{\text{reg}} = s_{\beta}(\mathbf{x})B + \underline{B} + \max\{0, \alpha_{\text{ex}}^{\eta} - \alpha_{\mathcal{L}_e}\}$ (see [1] for details). $\underline{B} > 0$ is a (small) baseline damping, the $B > \underline{B}$ is a larger damping coefficient for convergence. The switch $s_{\beta}(\mathbf{x})$ turns on close to the target; we model it as

$$s_{\beta}(\mathbf{x}) = \frac{1}{2} \left(\tanh(-\alpha_{\beta}(\|\mathbf{x}\| - r)) + 1 \right) \quad (1)$$

where $\alpha_{\beta} \in \mathbb{R}^+$ is a gain defining the switching rate, and $r \in \mathbb{R}^+$ is the radius where the switch is half-way engaged. And denoting the desired execution energy as $\mathcal{L}_e^{\text{ex,d}}$ we use the following policy for η

$$\eta = \frac{1}{2} \left(\tanh(-\alpha_{\eta}(\mathcal{L}_e^{\text{ex}} - \mathcal{L}_e^{\text{ex,d}}) - \alpha_{\text{shift}}) + 1 \right) \quad (2)$$

where $\alpha_{\eta}, \alpha_{\text{shift}} \in \mathbb{R}^+$ adjust the rate and offset, respectively, of the switch as an affine function of the speed error. Finally, α_{boost} is modeled as

$$\alpha_{\text{boost}} = k \eta (1 - s_{\beta}(\mathbf{x})) \frac{1}{\|\dot{\mathbf{x}}\| + \epsilon} \quad (3)$$

where $k \in \mathbb{R}^+$ is a gain that directly sets the desired level of acceleration, η (from above) sets $\alpha_{\text{boost}} = 0$ when the desired speed is achieved, and $1 - s_{\beta}(\mathbf{x})$ sets $\alpha_{\text{boost}} = 0$ when the system is within the region of higher damping. The normalization by $\|\dot{\mathbf{x}}\| + \epsilon$

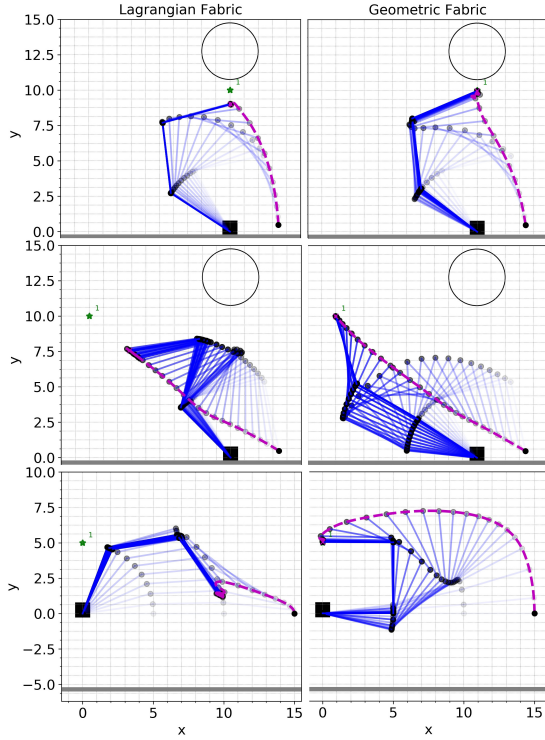


Fig. 1. Planar arm target reaching experiment results for Lagrangian fabric are shown in the left column and results for geometric fabric are shown in the right column, where targets are marked as green stars, and the arm’s alpha transparency ranges from light at the beginning of the trajectory to dark at the end.

ensures that α_{boost} is directly applied along $\hat{\mathbf{x}}$ with a very small positive value for ϵ to ensure numerical stability. This overall design injects more energy into the system when $-\alpha_{boost} < \alpha_{ex}^\eta - \alpha_{\mathcal{L}e}$. Since this injection occurs for finite time, the total system energy is still bounded. The additional switches ensure that the system is still subject to positive damping, guaranteeing convergence.

VII. PLANAR MANIPULATOR EXPERIMENTS

In this section, we run a set of controlled experiments on a 3-dof planar arm to show that geometric fabrics diminish potential fighting issues involved in baseline Lagrangian fabrics. The task objective here is to move the end-effector to a 2-D point target in different scenarios. To accomplish the task in each scenario, we build the system up layerwise following the empirically validated approach outlined in [arxiv paper]. In the first layer, We design policies that can generate the nominal behavior, including the target attraction policy that pulls the end-effector towards the target, the limit avoidance

policy that keeps each joint staying within its limit, and the default configuration policy that resolves the redundancy issue involved in 3-dof planar arm. In the second layer, we design policies that can shape the behavior as desired. Here, we add obstacle avoidance policy to the second layer of the fabric to avoid collision.

Here we focus on the geometric fabric descriptions and the only difference is that policies except for target attraction for geometric fabric are constructed as HD2 geometries, $\ddot{\mathbf{x}} = -\dot{\mathbf{x}}^2 \partial_{\mathbf{x}} \psi_1(\mathbf{x})$, while for Lagrangian fabric the policies are constructed as acceleration-based potentials, $\ddot{\mathbf{x}} = -\partial_{\mathbf{x}} \psi_1(\mathbf{x})$. Target attraction policy is constructed as acceleration-based potentials, $\ddot{\mathbf{x}} = -\partial_{\mathbf{x}} \psi_1(\mathbf{x})$ for both geometric fabric and Lagrangian fabric. Each policy is weighted by $\mathbf{M}(\mathbf{x})$ (or $\mathbf{M}(\mathbf{x}, \dot{\mathbf{x}})$) from a Finsler energy, $\mathcal{L} = \dot{\mathbf{x}}^T \mathbf{G}(\mathbf{x}) \dot{\mathbf{x}}$ (or $\mathcal{L} = \dot{\mathbf{x}}^T \mathbf{G}(\mathbf{x}, \dot{\mathbf{x}}) \dot{\mathbf{x}}$). For each policy, $\psi_1(\mathbf{x})$ and $\mathbf{G}(\mathbf{x})$ (or $\mathbf{G}(\mathbf{x}, \dot{\mathbf{x}})$) are defined in the following sections.

A. Limit Avoidance

To describe the joint limit avoidance policy, we use two task maps, $\mathbf{x} = \phi(\mathbf{q}_j) = \bar{\mathbf{q}}_j - \mathbf{q}_j$ and $\mathbf{x} = \phi(\mathbf{q}_j) = \mathbf{q}_j - \underline{\mathbf{q}}_j$, for each joint to capture the distance between the current joint position and its lower and upper boundaries, respectively, where $\bar{\mathbf{q}}_j$ and $\underline{\mathbf{q}}_j$ are the upper and lower limits of the j^{th} joint. The metric \mathbf{G}_l is defined as $\mathbf{G}_l(\mathbf{x}, \dot{\mathbf{x}}) = s(\dot{\mathbf{x}}) \frac{\lambda}{\dot{\mathbf{x}}}$ and where $s(\dot{\mathbf{x}})$ is a switching function, which takes the value of zero, if $\dot{\mathbf{x}} \geq 0$, takes the value of one, otherwise. Effectively, this removes the effect of the coordinate limit geometry once motion is orthogonal or away from the limit. The acceleration-based potential gradient, expressed as $\partial_{\mathbf{q}} \psi_l(\mathbf{x}) = M_l(\mathbf{x}) \partial_{\mathbf{q}} \psi_{1,l}(\mathbf{x})$, is designed with

$$\psi_l(\mathbf{x}) = \frac{\alpha_1}{\mathbf{x}^2} + \alpha_2 \log \left(e^{-\alpha_3(\mathbf{x}-\alpha_4)} + 1 \right) \quad (4)$$

where $\psi_l(\mathbf{x}) \rightarrow \infty$ as $\mathbf{x} \rightarrow 0$ and $\psi(\mathbf{x}) \rightarrow 0$ as $\mathbf{x} \rightarrow \infty$. Moreover, $\alpha_1, \alpha_2, \alpha_3, \alpha_4 \in \mathbb{R}^+$ where, α_1 and α_2 are gains that control the significance and mutual balance of the first and second terms. α_3 controls the sharpness of the smooth rectified linear unit (SmoothReLU) while α_4 offsets the SmoothReLU.

B. Default Configuration

The task map for default configuration policy is defined as $\mathbf{x} = \phi(\mathbf{q}) = \mathbf{q} - \mathbf{q}_0$, where \mathbf{q}_0 is a nominal configuration, and it usually represents the robot “at ready”. The metric \mathbf{G}_{dc} is simply an identity matrix scaled by a constant λ_{dc} , $\mathbf{G}_{dc} = \lambda_{dc} \mathbf{I}$.

The acceleration-based potential gradient, expressed as $\partial_{\mathbf{q}}\psi(\mathbf{x}) = M_{dc}(\mathbf{x})\partial_{\mathbf{q}}\psi_1(\mathbf{x})$, is designed with

$$\psi_1(\mathbf{x}) = k \left(\|\mathbf{x}\| + \frac{1}{\alpha_\psi} \log(1 + e^{-2\alpha_\psi\|\mathbf{x}\|}) \right) \quad (5)$$

where $k \in \mathbb{R}^+$ controls the overall gradient strength, $\alpha_\psi \in \mathbb{R}^+$ controls the transition rate of $\partial_{\mathbf{q}}\psi_1(\mathbf{x})$ from a positive constant to 0.

C. Obstacle Avoidance

We demonstrate collision avoidance with a circular object. The task map is $\mathbf{x} = \phi(\mathbf{y}) = \|\mathbf{y} - \mathbf{y}_o\| - r$, where \mathbf{y} , $\mathbf{y}_o \in \mathbb{R}^2$ are the current end-effector position and the origin of the circle in Euclidean space, and r is radius of the circle. The metric is defined as a function of position, $G_b(\mathbf{x}) = \frac{k_b}{\mathbf{x}^2}$, where $k_b \in \mathbb{R}^+$ is a barrier gain. The acceleration-based potential gradient, expressed as $\partial_{\mathbf{q}}\psi_b(\mathbf{x}) = M_b(\mathbf{x})\partial_{\mathbf{q}}\psi_{1,b}(\mathbf{x})$, is designed with $\psi_{1,b}(\mathbf{x}) = \frac{\alpha_b}{\mathbf{x}^8}$, where $\alpha_b \in \mathbb{R}^+$ is the barrier gain.

D. Target Attraction

To define target attraction policy that pulls the end-effector towards a target, we first introduce a task map, $\mathbf{x} = \phi(\mathbf{y}) = \mathbf{y} - \mathbf{y}_t$, where \mathbf{y} , $\mathbf{y}_t \in \mathbb{R}^2$ are the current end-effector position and the target position in Euclidean space. The metric is defined as

$$\mathbf{G}_\psi(\mathbf{x}) = (\bar{m} - \underline{m})e^{-(\alpha_m\|\mathbf{x}\|)^2}I + \underline{m}I. \quad (6)$$

where \bar{m} , $\underline{m} \in \mathbb{R}^+$ are the upper and lower isotropic masses, respectively, and $\alpha_m \in \mathbb{R}^+$ controls the width of the radial basis function. The acceleration-based potential gradient is defined in the same way as described in VII-B

E. Goal-reaching Experiment Results

Three tasks are performed in the controlled experiments on a 3-dof planar arm, which are described as follows. The first task is to reach a target near a circular obstacle, the second task is to reach a target located at the back of the planar arm, and the third task is to reach a target above the base. The first layer is applied in all three tasks to generate the nominal end effector behavior. On top that, we add the second layer with obstacle avoidance policy to the first and the second task for avoid collision. The nominal default configuration in all three tasks is chosen to be $[\frac{\pi}{2}, -\frac{\pi}{2}, -\frac{\pi}{2}]$, where positive sign defines counter clock-wise rotation, and negative sign defines clock-wise rotation. The upper and

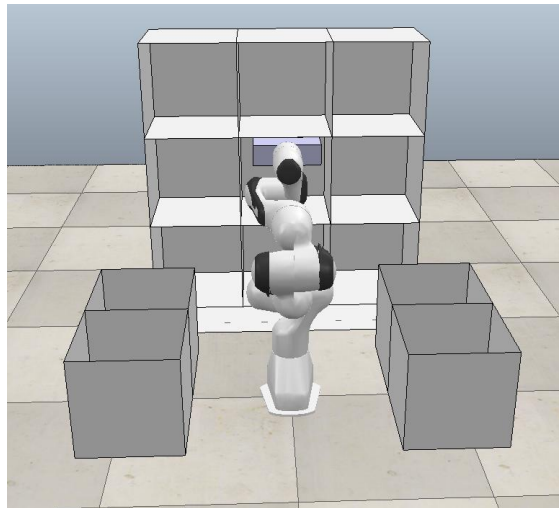


Fig. 2. Franka experiment scene.

lower joint limits are set to be $\pm(\pi)$ for each joint in the first two tasks and $\pm(\frac{\pi}{2} + 0.01)$ for each joint in task 3. We expect to see that baseline Lagrangian fabric is not capable of reaching the goal due to the potential fighting issue. However, geometric fabric diminishes this issue, and successfully reaches all three targets. The experiment results are shown in Fig. 1, From the top row to the bottom row, it shows the results of task 1 to task 3. From the left column, we can see that no target is reached due to the issue of fighting potentials between the target attraction and obstacle avoidance, default configuration, and joint limit avoidance. As we expected, all three targets are reached with geometric fabric as shown in the right column.

VIII. FRANKA ARM EXPERIMENTS

In this section, we run experiments on a 7-dof Franka arm, and show that geometric fabric scales to more complex settings. The experiments are performed in the environment shown in Fig. 2, where there are nine cubbies in front of the Franka arm, and two cubbies on each side of the arm. The length, width and depth of each cubby are 0.3m. The task objective is to continuously move the end effector to randomly selected targets located in different cubbies. To accomplish this task, we build the geometric fabric up layerwise as follows.

A. First Layer

In the first layer of the geometric fabric, we design policies that generates the nominal behavior

in the free space where no cubbies exists, and the objective is simply to move end effector to targets without exceeding joint limits or having redundancy issue. This can be done by adding the target attraction, the joint limit avoidance, and the default configuration, as described in VII-D, VII-A, and VII-B, respectively to the first layer. Instead of using one default configuration, here we have five default configuration candidates, and they are configurations with end-effector points to the left, the front left, the front, the front right and the right. The one has the end-effector pointing to the front is shown in Fig 2. We select the default configuration from the five candidates based on the proximity of the end-effector position in each default configuration and the target. To encourage straight-line motion in the end-effector task space, we add another target attraction policy to the first layer. This target attraction policy is similar to the one described in VII-D, but with a slight modification since it is formulated as a geometry, $\ddot{\mathbf{x}} = -\dot{\mathbf{x}}^2 \partial_{\mathbf{x}} \psi_1(\mathbf{x})$.

B. Second Layer

Once we get the desired nominal behavior, we design the second layer of the geometric fabric with a wall repulsion policy that can push the end effector out of the current cubby, and keep it away from the cubbies until it is in front of the target cubby.

The wall repulsion policy is described with two task maps. The first one is defined as the distance between the end effector and the back wall of the cubby, $\mathbf{x}_1 = \phi_1(\mathbf{y})$, where $\mathbf{y} \in \mathbb{R}^3$ is the current end-effector position in Euclidean space. The second task map is defined as the distance between the end-effector and a cylinder, whose center line is orthogonal to the back wall of the target cubby while passing by the center of the target cubby, $\mathbf{x}_2 = \phi_2(\mathbf{y})$, where $\mathbf{y} \in \mathbb{R}^3$ is the current end-effector position in Euclidean space. The radius of the cylinder is half of the cubby size, which is $0.15m$. The priority metric is defined in the way such that the priority vanishes if the end-effector is either more than $d = 0.4m$ away from the back wall of the cubby or it is inside of the cylinder aligned with the target cubby, specifically:

$$\mathbf{G}_w(\mathbf{y}) = s(\mathbf{x}_1)((\bar{m} - \underline{m})\mathbf{T}(\mathbf{x}_2) + \underline{m})I. \quad (7)$$

where $s(\mathbf{x}_1)$ is a range-based switching function. Specifically, $s(\mathbf{x}_1) = 1$ if $\mathbf{x}_1 < d$ and $s(\mathbf{x}_1) =$

0, otherwise. $\mathbf{T}(\mathbf{x}_2) = \tanh(-(\alpha_m \|\mathbf{x}_2\|)^2 + 1)$, where $\bar{m}, \underline{m} \in \mathbb{R}^+$ are the upper and lower isotropic masses, respectively, and $\alpha_m \in \mathbb{R}^+$ defines the width of the transition between 0 and 1. The acceleration-based potential gradient and policy formulation are the same as described in VII-A

To help pulling the end-effector to the target inside a cubby, we design another target attraction policy in this layer, which is similar to the one defined in Section VII-D, but with some modification in both the priority metric and the policy formulation. The metric is designed with the same formula as in Eq. 7 but complimentary to the metric for wall repulsion policy, meaning the priority remains zero until it enters the cylinder aligned with the target cubby.

C. Third Layer

Once we get the desired behavior, we add a cubby repulsion policy to the third layer of the fabric for collision avoidance. The cubby repulsion policy is the same as the circular object repulsion defined in Section VII-C, except for a slightly different definition of the task map. To describe the cubby repulsion policy, we use a one-dimensional task space $\mathbf{x} = \phi(\mathbf{y})$ to capture the minimum distance between a point on the arm and the cubby, where $\mathbf{y} \in \mathbb{R}^3$ is the coordinates of a point on the robot. If the point is inside of a cubby, the minimum distance is between the point and one of the walls of the cubby. Otherwise, the minimum distance is between the point and one of the edges of the cubby.

D. Cubby Experiment Results

We generate a random set of targets, and run simulation with three different settings. First, we run simulation with only the first layer of the geometric fabric. Next, we run simulation with the addition of the second layer to the fabric. Last, we run simulation with the geometric fabric with all three layers. We demonstrate the simulation results with video clips presented in our website <https://sites.google.com/nvidia.com/geometric-fabrics>. As we designed, the first layer of the geometric fabric generates the nominal behavior, which simply moves the end-effector to each target in the free space. With the default configuration policy, the robot always moves around its front side. In the first video clip, we can observe that the robot moves from the cubby on its left side to the cubby on its right side around its

front instead of its back. With the addition of the second layer, the geometric fabric generates motion that moves the end-effector out of the current cubby first, and then approaches to the target after it enters the target cubby, as shown in the second video clip. With all three layers, the geometric fabric generates motion that moves the end-effector to targets located in different cubbies continuously while preventing the robot from colliding with the cubby, as shown in the third video clip.

REFERENCES

- [1] N. D. Ratliff, K. V. Wyk, M. Xie, A. Li, and A. M. Rana, “Generalized nonlinear and finler geometry for robotics,” *arXiv preprint arXiv:(in prep)*, 2020.
- [2] C.-A. Cheng, M. Mukadam, J. Issac, S. Birchfield, D. Fox, B. Boots, and N. Ratliff, “RMPflow: A computational graph for automatic motion policy generation,” in *The 13th International Workshop on the Algorithmic Foundations of Robotics*, 2018.
- [3] F. Bullo and A. D. Lewis, *Geometric control of mechanical systems: modeling, analysis, and design for simple mechanical control systems*. Springer Science & Business Media, 2004, vol. 49.
- [4] O. Khatib, “A unified approach for motion and force control of robot manipulators: The operational space formulation,” *IEEE Journal of Robotics and Automation*, vol. 3, no. 1, pp. 43–53, 1987.
- [5] J. Peters, M. Mistry, F. Udwadia, J. Nakanishi, and S. Schaal, “A unifying framework for robot control with redundant DOFs,” *Autonomous Robots*, vol. 24, no. 1, pp. 1–12, 2008.
- [6] S. M. LaValle, *Planning Algorithms*. Cambridge, U.K.: Cambridge University Press, 2006, available at <http://planning.cs.uiuc.edu/>.
- [7] D. Kappler, F. Meier, J. Issac, J. Mainprice, C. Garcia Cifuentes, M. Wüthrich, V. Berenz, S. Schaal, N. Ratliff, and J. Bohg, “Real-time perception meets reactive motion generation,” *IEEE Robotics and Automation Letters*, vol. 3, no. 3, pp. 1864–1871, Jul. 2018. [Online]. Available: <https://arxiv.org/abs/1703.03512>
- [8] N. Ratliff, M. Toussaint, and S. Schaal, “Understanding the geometry of workspace obstacles in motion optimization,” in *IEEE International Conference on Robotics and Automation (ICRA)*, 2015.
- [9] M. Mukadam, J. Dong, X. Yan, F. Dellaert, and B. Boots, “Continuous-time Gaussian process motion planning via probabilistic inference,” *International Journal of Robotics Research (IJRR)*, vol. 37, no. 11, pp. 1319–1340, 2018.
- [10] T. Erez, K. Lowrey, Y. Tassa, V. Kumar, S. Kolev, and E. Todorov, “An integrated system for real-time model-predictive control of humanoid robots,” in *IEEE/RAS International Conference on Humanoid Robots*, 2013.
- [11] N. D. Ratliff, J. Issac, D. Kappler, S. Birchfield, and D. Fox, “Riemannian motion policies,” *arXiv preprint arXiv:1801.02854*, 2018.
- [12] M. A. Rana, A. Li, H. Ravichandar, M. Mukadam, S. Chernova, D. Fox, B. Boots, and N. Ratliff, “Learning reactive motion policies in multiple task spaces from human demonstrations,” in *Conference on Robot Learning (CoRL)*, 2019.
- [13] M. Mukadam, C.-A. Cheng, D. Fox, B. Boots, and N. Ratliff, “Riemannian motion policy fusion through learnable lyapunov function reshaping,” in *Conference on Robot Learning (CoRL)*, 2019.
- [14] A. Li, M. Mukadam, M. Egerstedt, and B. Boots, “Multi-objective policy generation for multi-robot systems using riemannian motion policies,” *CoRR*, vol. abs/1902.05177, 2019. [Online]. Available: <http://arxiv.org/abs/1902.05177>
- [15] J. M. Lee, *Introduction to Smooth Manifolds*, 2nd ed. Springer, 2012.
- [16] L. Righetti, M. Kalakrishnan, P. Pastor, J. Binney, J. Kelly, R. Voorhies, G. Sukhatme, and S. Schaal, “An autonomous manipulation system based on force control and optimization,” *Autonomous Robots*, 2013.
- [17] N. D. Ratliff, K. V. Wyk, M. Xie, A. Li, and A. M. Rana, “Generalized nonlinear and finler geometry for robotics,” *arXiv preprint arXiv:(in prep)*, 2020.
- [18] C.-A. Cheng, M. Mukadam, J. Issac, S. Birchfield, D. Fox, B. Boots, and N. Ratliff, “Rmpflow: A computational graph for automatic motion policy generation,” *arXiv preprint arXiv:1811.07049*, 2018.